Intermediate nonlinear regime of a line-tied g mode

P. Zhu, C. C. Hegna, and C. R. Sovinec
Center for Plasma Theory and Computation
University of Wisconsin-Madison
Madison, WI 53706

A. Bhattacharjee and K. Germaschewski
Space Science Center and the Center for Magnetic Self-Organization
University of New Hampshire
Durham, NH 03824

Abstract

A sequence of nonlinear regimes are identified for the nonlinear development of a line-tied g-mode. The dynamics of the intermediate nonlinear regime is described. This regime is operable when the mode's convection amplitude is comparable to the mode width in the direction of the density gradient. The governing equations are derived. Comparisons between these equations and direct MHD simulations show excellent agreement.

I. INTRODUCTION

The gravitational (g) mode is a term used in fusion community for the magnetic Rayleigh-Taylor instability. It is driven by having an equilibrium with a density gradient in the opposite direction of the gravity vector. Because of its simpler geometry, a line-tied g mode is often used to model the phenonomena in magnetic plasmas that involve pressure-driven instabilities, such as the edge localized modes (ELMs) in tokamaks and the substorm onset in Earth's magnetotail. A primary motivation for us to study a line-tied g mode here is to understand the nonlinear ELMs.

Due to its potential damages to the first wall and divertor target of a tokamak, the ELM is a major concern for next generation experiments, such as ITER, which is going to operate in H-mode with high-β and high fraction of bootstrap current driven by large pressure gradient in the edge. Over last decade, it has become well accepted that the onset of ELMs in tokamaks is due to the breaching of peeling-ballooning instability boundaries of the edge pedestal region [1, 2]. The filament structures observed in experiments [3] and direct MHD simulations [4] indicate that the ballooning structure continues to dominate in the nonlinear stage of ELMs. In order to understand the nonlinear behavior of ELMs, it is crucial to address the following questions about the nonlinear ballooning instability. What is the major and most relevant nonlinear regime? What is the nonlinear growth rate and saturation magnitude?

The answers to those questions may be addressed through the study of line-tied g modes. These modes are geometrically simpler than ballooning instabilities in torii. Nonetheless, there are considerable similarities between these two phenomena. The Rayleigh-Taylor drive $\mathbf{g} \cdot \nabla\rho$ can be used to model the interchange force, and the line-tying boundary condition introduces small but finite wavenumber parallel to magnetic field hence line-bending force. Thus a line-tied g mode may serve as a prototype model for the ballooning instability.

We consider the g mode in a shearless slab configuration of line-tied flux tubes (Fig. 1) where magnetic field lines support plasma against a constant gravity $\mathbf{g}$. A Cartesian coordinate system is adopted, with $\hat{\mathbf{x}}$, $\hat{\mathbf{y}}$, and $\hat{\mathbf{z}}$ being the basis vectors. The equilibrium field $\mathbf{B}_0$ are tied to two ends in the direction of $\hat{\mathbf{z}}$; the gradients of equilibrium density ρ_0 and pressure p_0 are in the direction of $\hat{\mathbf{x}}$ perpendicular to field lines, and the gravity $\mathbf{g}$ is in the direction of $-\hat{\mathbf{x}}$; we study modes that varies rapidly in the y-direction, which is perpendicular to both

equilibrium field lines and density gradient (as well as gravity). Specifically, we have

$$\rho_0 = \rho_0(x_0), \quad p_0 = p_0(x_0), \quad \mathbf{B}_0 = B_0(x_0)\hat{\mathbf{z}}, \quad \mathbf{g} = -g\hat{\mathbf{x}}, \tag{1}$$

with the equilibrium satisfying

$$\frac{d}{dx_0}\left(p_0 + \frac{B_0^2}{2}\right) = -\rho_0 g.$$

Here, $\mathbf{r}_0 = x_0\hat{\mathbf{x}} + y_0\hat{\mathbf{y}} + z_0\hat{\mathbf{z}}$ denotes the initial location of each plasma element in the equilibrium. Here and in the rest of the paper, CGS units are used and a 4π factor has been absorbed in ρ_0 and p_0. The particular equilibrium used is a one dimensional hypertangential profile for density $\rho_0(x_0) = \rho_c + \rho_h \tanh(x_0 - x_c)/L_\rho$, and pressure $p_0(x_0) = \rho_0(x_0)$, with x_c and L_ρ modeling the center location and the width of the pedestal; ρ_c and ρ_h representing the average density and (half) height of the pedestal.

The model pedestal equilibrium considered here is most unstable to the line-tied g modes that vary rapidly in the y-direction. In the nonlinear regimes of those modes, there are two small parameters

$$\epsilon \sim \frac{|\boldsymbol{\xi}|}{L_z} \ll 1, \qquad n^{-1} \sim \frac{k_\parallel}{k_\perp} \sim \frac{L_y}{L_z} \ll 1, \tag{2}$$

and the plasma displacement is expanded in terms of those two small parameters in the following form

$$\boldsymbol{\xi}(\sqrt{n}x_0, ny_0, z_0, t) = \sum_{i=1}^{\infty}\sum_{j=0}^{\infty} \epsilon^i n^{-\frac{j}{2}} \left(\hat{\mathbf{x}}\xi_{x\{i,j\}} + \frac{\hat{\mathbf{y}}}{\sqrt{n}}\xi_{y\{i,j\}} + \hat{\mathbf{z}}\xi_{z\{i,j\}}\right). \tag{3}$$

Here, we define the perturbation spatial scales $x = \sqrt{n}x_0$, $y = ny_0$, $z = z_0$; L_z denotes the length of the equilibrium flux tubes in z direction; L_y is the wavelength of the perturbation in y direction, and $k_\parallel$ and $k_\perp$ the dominant wavenumber of perturbation parallel and perpendicular to equilibrium magnetic field lines respectively. We use L_z as the normalization length scale in this paper so that $L_z = 1$. The relative magnitudes of the three components of the displacement vector are chosen in accordance with conventional linear theory on ballooning modes [5, 6]. Recent direct simulations have indicated that such an ordering still holds in the early to intermediate nonlinear phases of the g-mode evolution [7].

A Lagrangian formulation of the ideal MHD equations is used for expansion and analysis [8]. In particular, the equation of motion is written as

$$\frac{\rho_0}{J}\nabla_0\mathbf{R}\cdot\frac{\partial^2\boldsymbol{\xi}}{\partial t^2} = -\nabla_0\left[\frac{p_0}{J^\gamma} + \frac{(\mathbf{B}_0\cdot\nabla_0\mathbf{R})^2}{2J^2}\right] + \nabla_0\mathbf{R}\cdot\left[\frac{\mathbf{B}_0}{J}\cdot\nabla_0\left(\frac{\mathbf{B}_0}{J}\cdot\nabla_0\mathbf{R}\right)\right] + \frac{\rho_0}{J}\nabla_0\mathbf{R}\cdot\mathbf{g} \tag{4}$$

where

$$\mathbf{R}(\mathbf{r}_0, t) = \mathbf{r}_0 + \boldsymbol{\xi}(\mathbf{r}_0, t), \quad \nabla_0 = \frac{\partial}{\partial \mathbf{r}_0}, \quad J(\mathbf{r}_0, t) = |\nabla_0 \mathbf{R}|,$$

and $\boldsymbol{\xi}(\mathbf{r}_0, 0) = 0$. As will see next, such an expansion allows us to analyze the growth and structure of various linear and nonlinear regimes of the line-tied g-mode.

The rest of paper is organized as follows. In Sec. II, we show that the usual linear ballooning theory is reproduced for the line-tied g-mode with this formalism. (For brevity, we refer to the ballooning-like, line-tied g-mode as ballooning-g mode in the rest of the paper.) In Sec. III, we describe the first nonlinear regime of the ballooning-g mode evolution and compare the earlier theory prediction based on the analysis of this regime with direct MHD simulations. We introduce the second, intermediate nonlinear regime in Sec. IV, where the governing equations for that regime are derived and solved. The solutions are compared with results from direct MHD simulations. Finally, summary and discussions are given in Sec. V.

II. LINEAR MODE STRUCTURE

In the first order expansion in ϵ we recover the linear mode equations. To the leading order of $n^{-1/2}$ ($\mathcal{O}(n^0)$), with an eikonal approximation $\boldsymbol{\xi} \sim \exp(-ik_y y)$, where $k_y L_z \sim n \gg 1$, we have the local eigenmode equations (aligned along each field line at a given x_0) follow from the x and z component of the above force operator expansions:

$$\partial_t^2 \xi_{x\{1,0\}} = \Gamma_{\rm A}^2 \partial_z^2 \xi_{x\{1,0\}} + \left[\frac{g}{L_\rho} + \frac{g^2}{\Gamma_{\rm A}^2(1+\gamma\beta)}\right] \xi_{x\{1,0\}} + \frac{g}{1+\gamma\beta} \partial_z \xi_{z\{1,0\}}, \tag{5}$$

$$\partial_t^2 \xi_{z\{1,0\}} = \frac{c_s^2}{1+\gamma\beta} \partial_z^2 \xi_{z\{1,0\}} - \frac{g}{1+\gamma\beta} \partial_z \xi_{x\{1,0\}}, \tag{6}$$

where $\Gamma_{\rm A}^2 = B^2/\rho$, $L_\rho = \rho/\rho'$, $c_s^2 = \gamma p/\rho$, and $\beta = p/B^2$. The two coupled eigenmode equations strongly resemble those for a linear ballooning mode in a curved magnetic field [5, 6]. It is worth noting that linear ballooning-like eigenmodes always involve plasma and magnetic compressions. Only near marginal stability when $\tau_{\rm A}^2 \partial_t^2 \ll 1$ will compressional effects be negligible (here $\tau_{\rm A} = \sqrt{\rho}/B = \Gamma_{\rm A}^{-1}$ denotes the time that it takes a local shear Alfvén wave traveling a unit distance along the equilibrium magnetic field). However, for closed field lines, and for field lines with line-tied boundary condition, plasma compression cannot be ignored near marginal stability. In those cases, the coupled eigenmode equations

in (5) and (6) reduce to a single differential-integral eigenmode equation for $\xi_{x\{1,0\}}$ [9]

$$\partial_z^2 \xi_{x\{1,0\}} + \left(\frac{g}{L_\rho \Gamma_{\rm A}^2} + \frac{g^2}{c_s^2 \Gamma_{\rm A}^2} \right) \xi_{x\{1,0\}} - \frac{g^2}{c_s^2 \Gamma_{\rm A}^2} \frac{\left\langle \xi_{x\{1,0\}} \right\rangle}{1+\gamma\beta} = \frac{\Gamma^2}{\Gamma_{\rm A}^2} \xi_{x\{1,0\}} \simeq 0, \tag{7}$$

and a solution for $\xi_{z\{1,0\}}$

$$\xi_{z\{1,0\}} = \frac{g}{c_s^2} \int_0^z dz' \left(\xi_{x\{1,0\}} - \left\langle \xi_{x\{1,0\}} \right\rangle \right), \tag{8}$$

where

$$\left\langle \xi_{x\{1,0\}} \right\rangle \equiv \frac{1}{L_z} \int_0^{L_z} dz \xi_{x\{1,0\}}$$

is the average over the domain $0 < z < L_z$ and $\Gamma(x_0)$ is the local eigenvalue (growth rate) along each field line. The local eigenmode equations in Eqs. (5)-(6) or in Eq. (7) only determine the mode structure along each field line. Consider the marginal stability case where $\Gamma^2/\Gamma_{\rm A}^2 \sim \mathcal{O}(n^{-1})$, and denote Eq. (7) as $\mathcal{L}H(z) = (\Gamma^2/\Gamma_{\rm A}^2)H(z)$. The structure of the global mode takes the form

$$\xi_{x\{1,0\}} = \xi_{x(1)}(x,y,\tau) H(z), \quad (\tau = n^{-\frac{1}{2}} t). \tag{9}$$

At next two orders of $n^{-1/2}$, we recover the envelope equation with the Connor-Hastie-Taylor global ballooning mode structure [5]

$$\frac{C_0}{\Gamma_{\rm A}^2} \partial_\tau^2 \partial_y^2 \xi_{x(1)} = C_1 \frac{n\Gamma^2}{\Gamma_{\rm A}^2} \partial_y^2 \xi_{x(1)} + C_2 \partial_x^2 \xi_{x(1)}, \tag{10}$$

where

$$C_0 = \left\langle H^2 \right\rangle + \frac{g^2}{c_s^4} \left\langle \left(\int_0^z dz' \left(H - \langle H \rangle \right) \right)^2 \right\rangle, \tag{11}$$

$$C_1 = \left\langle H^2 \right\rangle, \tag{12}$$

$$C_2 = -\left\langle (H')^2 \right\rangle, \tag{13}$$

and $H' \equiv dH/dz$. With proper boundary conditions, such as solid wall boundary conditions in x and periodic boundary conditions in y, the above envelope equation determines the global eigenmode structure as well as the global eigenvalue, which is given by the maximum of $\Gamma^2(x_0)$ with $\mathcal{O}(n^{-1})$ stabilizing corrections.

Like the ballooning instability, there are three spatial scales in the structure of the linear line-tied g mode, basically, the mode width in the direction of $\hat{\mathbf{z}}$, $\hat{\mathbf{x}}$, and $\hat{\mathbf{y}}$ along, across, and perpendicular to field lines, respectively. If we denote the mode width in each Cartesian

direction as l_i $(i = x, y, z)$, the ratio of these three scales can be expressed in terms of n as follows

$$l_z : l_x : l_y = 1 : \frac{1}{\sqrt{n}} : \frac{1}{n}.$$

The multiple scales involved bring considerable complexity and difficulty, such as anisotropy and stiffness, to the nonlinear analysis of the mode in simulations. On the other hand, such a separation of spatial scales provides a natural measure of the nonlinear regimes of the line-tied g mode in theory.

As the g-mode grows from linear to nonlinear phase, its amplitude ϵ can be measured by the ballooning scales $n^{-\frac{j}{2}}$ in the decreasing sequence of $j = \infty, \cdots, 3, 2, 1, \cdots$. When the mode acquires the absolute order of $\epsilon = n^{-1}$, it enters a regime that was first derived by Cowley and Artun [9], denoted as the Cowley-Artun (CA) regime in the following. As the mode continues to grow nonlinearly, the mode amplitude will increase to the order of $\epsilon = n^{-1/2}$. We denote this regime as intermediate nonlinear regime. In next two sections, we focus our discussions on these two nonlinear regimes, as well as the transition of the nonlinear g-mode from CA regime to intermediate regime.

III. $\epsilon \sim n^{-1}$: EARLY NONLINEAR REGIME

When $\epsilon \sim n^{-1}$, the mode convection in x direction is of the order of the mode width in y diretion; that is, $\xi_x \sim l_y \sim L_z/n$. In this regime, the Jacobian is unity and the Lagrangian compression $\nabla_0 \cdot \boldsymbol{\xi} = 0$ to leading order, hence

$$J_{\{1,-1\}} = \partial_x \xi_{x\{1,0\}} + \partial_y \xi_{y\{1,0\}} = 0. \tag{14}$$

The local eigenvalue equation for $\xi_{x\{1,0\}}$ remains the same as in the linear case, so that

$$\xi_{x\{1,0\}} = \xi_{x(1)}(x, y, \tau) H(z). \quad (\tau = n^{-\frac{1}{2}} t) \tag{15}$$

The dominant nonlinear effects modify the linear envelope equation in (10) and yield a new equation with two extra nonlinear terms that were previously derived in [9]

$$\frac{C_0}{\Gamma_{\rm A}^2} \partial_y^2 \partial_\tau^2 \xi_{x(1)} = C_1 \frac{n\Gamma^2}{\Gamma_{\rm A}^2} \partial_y^2 \xi_{x(1)} + C_2 \partial_x^2 \xi_{x(1)} + C_3 \partial_x^2 \overline{\xi_{x(1)}^2} \partial_y^2 \xi_{x(1)} + C_4 \partial_y^2 \xi_{x(1)}^2 \tag{16}$$

where $\bar{A} \equiv L_y^{-1} \int_0^{L_y} dy A$ is the average over domain $0 < y < L_y$. The coefficients C_i $(i = 0, \cdots, 4)$ are determined by the equilibrium configuration and linear mode structure

along field lines. In particular, the coefficients of the linear terms, C_0, C_1, and C_2, are the same as in the linear envelope equation (10), as given in (11) to (13). The coefficients of the nonlinear terms, C_3 and C_4, are listed in [9, 10]. The Cowley-Artun regime as governed by Eq. (16) is characterized by two orderings: $\Gamma^2/\Gamma_{\rm A}^2 \sim \mathcal{O}(n^{-1})$, and $\epsilon \sim n^{-1}$ (see Table I). The former ordering is a measure of the distance of the equilibrium away from marginal stability. The latter ordering holds when convection is small relative to the mode spatial scales, i.e. $\boldsymbol{\xi}\cdot\nabla \sim n^{-\frac{1}{2}} \ll 1$. Eq. (16) predicts a "finite-time-like" singular solution when the nonlinear term $C_4\partial_y^2\xi_{x(1)}^2$ becomes dominant. Crudely, when this occurs the displacement scales as $\xi_{x(1)} \sim (t_s - t)^{-a}$ with $t_s > 0$ and $a > 0$ (where t_s is the time when the singularity occurs)n [9]. The detonation regime where the C_4 nonlinear term dominates and the finite-time singular solution exists may be specified as follows:

$$\frac{C_1\Gamma^2}{C_4\Gamma_{\rm A}^2} \ll \xi_x \ll \mathcal{O}(n^{-\frac{1}{2}}), \tag{17}$$

where $\xi_x = \boldsymbol{\xi}\cdot\hat{\mathbf{x}}$ is the x component of the plasma displacement and the second inequality marks the regime of validity for Eq. (16).

Direct MHD simulations of g-mode have been carried out recently in both a finite difference code (called BIC, which stands for Ballooning-Interchange Code and was developed at University of New Hampshire) [7] and the NIMROD code [11]. (The details of the simulation settings are described in [7, 10].) In both cases, all MHD field components remain bounded in magnitude throughout the intermediate nonlinear phase. The growth rates in the nonlinear phase are only slightly lower than that in the linear phase. there is not a distinctive detonation regime where a faster than exponential growth can be observed in those particular simulations. This nearly exponential (or "linear") growth occurs despite the fact that theory indicates that nonlinearities are relevant to the amplitude evolution. It is possible that the equilibria in those simulations are not sufficiently close to marginal stability as required for a substantial presence of the detonation regime. It remains a challenge to pursue the detonation regime of nonlinear g-mode in direct MHD simulations. Nevertheless, it seems that the "finite-time-like" singular growth is not a generic feature of nonlinear g-mode evolution.

While the CA regime does predict explosive growth, at sufficient amplitude of the displacement the envelop evolution equation is no longer valid for fixed $n \gg 1$. Rather, nonlinear growth enters another nonlinear stage. The issue is then to correctly predict the mode

structure and growth as it preceeds through various stages of nonlinear evolution. In particular, the question of faster than linear growth is of central importance. The detonaton regime, as crudely characterized in Eq. (17), in practice may be a narrow regime of applicability, depending upon the proximity of the equilibrium to instability boundries. What these bounds suggest is that an MHD equilibrium that evolves "quickly" through marginal stability will not experience a distinctive disruptive stage with fast nonlinear growth.

IV. $\epsilon \sim n^{-1/2}$: INTERMEDIATE NONLINEAR REGIME

Direct MHD simulation results clearly show the transition from the $\epsilon \sim n^{-1}$ regime to the $\epsilon \sim n^{-1/2}$ regime. For the direct MHD simulation case shown in Fig. 2, $n = 1280 \gg 1$, $n^{-1} = 0.0008$ and $n^{-\frac{1}{2}} \sim 0.03$, respectively. Since the linear growth rate $\Gamma \sim 0.08$ ($\Gamma^2/\Gamma_{\rm A}^2 \sim 0.0008$) and $\xi_x \sim u_x/\Gamma$, the CA regime and the intermediate regime in terms of velocity amplitude are approximately $u_x \sim 0.008$ and $u_x \sim 0.3$, respectively. The three vertical broken lines in Fig. 2a mark the three time slices where the pressure contours in $x - y(z = 0)$ plane are plotted in Fig. 2b. The first two time slices, t_1 and t_2, basically correspond to the CA regime and the intermediate nonlinear regime respectively. When $t \sim t_1 \sim 46$ in CA regime, $\xi_x \sim L_z/n \sim 0.1 \sim l_y$ where l_y is the mode width in y direction (and $L_z = 128$ in simualtions). Since $\xi_x \sim l_y \ll L_\rho = 5$, the distortion of equilibrium pressure contour in $x - y(z = 0)$ plane and equilibrium pressure profile along $y = z = 0$ line is barely noticable in Fig. 2b. When $t \sim t_2 \sim 80$ in the intermediate nonlinear regime, $\xi_x \sim L_z/\sqrt{n} \sim 3.6 \sim l_x$ where l_x is the mode width in x direction. During this phase $\xi_x \sim l_x \sim L_\rho = 5$, the finger pattern in pressure contour becomes apparant in $x - y(z = 0)$ plane and the pressure profile along $y = z = 0$ line starts to steepen as shown in Fig. 2b.

The intermediate nonlinear regime of a line-tied g mode is defined by the ordering that $\epsilon \sim n^{-1/2}$ or $\xi_x \sim l_x$, when the convection in x direction reaching the order of mode width in the same x direction, which is the intermediate scale of the linear mode spatial structure. Close to marginal stability, the mode width l_x could approach the density/pressure gradient scale length in the pedestal region. Thus plasma convection in this regime is capable of configurating the entire pedestal region in x direction. The relation between the CA regime and the intermediate nonlinear regime may be summarized in Table I.

The governing equations for the intermediate nonlinear regime have recently been de-

TABLE I: Linear and Nonlinear regimes of a line-tied g-mode

	$\Gamma^2/\Gamma_{\rm A}^2 \sim \mathcal{O}(n^{-1})$	$\Gamma^2/\Gamma_{\rm A}^2 \sim \mathcal{O}(n^{-\frac{1}{2}})$	$\cdots$
$\epsilon \ll n^{-1}$	linear regime		
$\epsilon \sim n^{-1}$	Cowley-Artun regime		
$\epsilon \sim n^{-\frac{1}{2}}$	intermediate nonlinear regime		
$\vdots$			

rived [10]. In this regime, the leading order Lagrangian compression, which is proportional to $\partial_x \xi_{x(0)} + \partial_y \xi_{y(0)}$, is no longer zero in general due to enhanced nonlinearity, as it was in CA regime. The governing equaion for the CA regime in Eq. 16, which was valid when $\epsilon \sim n^{-1}$ and critically dependent on the condition that the leading order Lagrangian compression being zero, no longer applies in this intermediate nonlinear regime.

In contrast to the CA regime, where nonlinearity only modifies the envelope equation, in the intermediate nonlinear regime, nonlinearity directly modifies the evolution of the x component of the local ballooning-like g-mode equations, whereas the equation for the z-component remains the same as linear theory. If we denote the linear local eigenmode equations in Eqs. (5) and (6) for the line-tied g-mode as

$$\partial_t^2 \xi_{x(0)} = \mathcal{L}_x(\xi_{x(0)}, \xi_{z(0)}), \tag{18}$$

$$\partial_t^2 \xi_{z(0)} = \mathcal{L}_z(\xi_{x(0)}, \xi_{z(0)}), \tag{19}$$

the governing equations for the intermediate nonlinear regime ($\epsilon \sim n^{-1/2}$) can be written in the form

$$\begin{aligned} &\partial_y \left(\partial_t^2 \xi_{x(0)} - \mathcal{L}_x(\xi_{x(0)}, \xi_{z(0)}) \right) + [\xi_{x(0)}, \partial_t^2 \xi_{x(0)}] \\ &\quad = \frac{g}{1+\gamma\beta} [\xi_{x(0)}, \partial_z \xi_{z(0)}] + \Gamma_{\rm A}^2 [\xi_{x(0)}, \partial_z^2 \xi_{x(0)}], \end{aligned} \tag{20}$$

$$\partial_t^2 \xi_{z(0)} = \mathcal{L}_z(\xi_{x(0)}, \xi_{z(0)}) \tag{21}$$

which are subject to the no-slip, solid wall boundary condition at $x = 0, L_x$, line-tying boundary condition at $z = 0, L_z$, and periodic boundary condition in y. Here $[A, B] \equiv \partial_x A \partial_y B - \partial_x B \partial_y A$.

The intermediate nonlinear equations in Eqs. (20) and (21) have been solved numerically. We solve those two coulpled nonlinear equations with the same initial-boundary conditions

as those used in a corresponding direct MHD simulation. The growth of the maximum of the x-component of the flow ($u_x = \partial_t \xi_x$) obtained from both the numerical solution and the MHD simulation are plotted in Fig. 3. The prediction from theory agrees with the result from simulation throughout linear and nonlinear phase. The transition from the CA regime ($\epsilon \sim n^{-1}$) to the intermediate regime ($\epsilon \sim n^{-1/2}$) is well reproduced with the solution of the intermediate nonlinear equations. This case has a relatively short linear phase ($30 \lesssim t \lesssim 40$) because the initial flow magnitude ($u_{x0} = 10^{-3}$) is not well below the CA regime ($u_x^{\rm CA} \sim 0.008$).

Shown in Fig. 4 is a case of comparison where the simulation is initialized with a smaller perturbation of flow, $u_{x0} = 10^{-5}$, whereas the rest of conditions remain the same as the previous case. In this case, there is a substantial phase of linear growth before the CA nonlinear regime is reached. After an initial transient phase, the theory and MHD simulations show excellent agreement in the linear and subsequent early and intermediate nonlinear phases. Fig. 4 also shows the agreement for the z-component of the flow (u_z) in those linear and nonlinear phases between theory and simulation.

These comparisons indicate that the transition from CA regime to intermediate nonlinear regime can be well represented by the intermediate nonlinear equations. The intermediate nonlinear regime appears to be the major and more relevant nonlinear regime of the development of a line-tied g mode. The intermediate regime is further developed into late nonlinear phase. In the simulation case shown in Fig. 2, the beginning of the late nonlinear phase corresponds to the time around $t = t_3$, which is marked by the formation of a fully developed thin finger pattern in the $x - y$ projection of pressure contour, and a shock-like discontinuous structure in the pressure profile along the line $y = z = 0$.

V. SUMMARY AND DISCUSSION

In summary, an intermediate regime has been identified for the nonlinear development of a line-tied g mode in both theory and simulations. This regime is entered when the radial displacement is of order the mode width in the direction of the equilibrium density gradient. The g-mode proceeds through a sequence of phases as measured by the strength of the nonlinearity relative to n^{-1} ($\epsilon \ll n^{-1}$, $\epsilon \sim n^{-1}$, $\epsilon \sim n^{-1/2}$, etc., where $\epsilon \sim |\boldsymbol{\xi}|/L_{\rm z}$ is the mode amplitude normalized by the length of equilibrium flux tubes, and $n \sim k_\perp/k_\parallel$ is the ratio of

wavenumbers along and perpendicular to equilibrium magnetic field). For equilibria that are close to linear marginal stability [$\Gamma^2/\Gamma_A^2 \sim \mathcal{O}(n^{-1})$], the Cowley-Artun regime is recovered in early nonlinear phase when $\epsilon \sim n^{-1}$, i.e. the plasma convection in the x direction grows to the order of the mode width in the y direction ($\xi_x \sim l_y$). In this regime, the lowest order Lagrangian compression $\nabla_0 \cdot \boldsymbol{\xi}$ is zero. The local mode structure along each field line remains the same as in linear regime; nonlinearity modifies the envelop equation of the linear global mode. As the plasma convection in the x direction grows to the order of mode width in the same x direction ($\xi_x \sim l_x$), the nonlinearity is enhanced to the ordering $\epsilon \sim n^{-1/2}$ and enters the intermediate nonlinear regime. In this regime, the leading order Lagrangian compression is no longer zero [$\nabla_0 \cdot \boldsymbol{\xi} \sim \mathcal{O}(1)$] and the governing equation in Eq. (16) for Cowley-Artun regime no longer applies. During this phase, nonlinearity directly modifies the growth and structure of linear local modes. Sound wave physics becomes present and important, as indicated by stronger coupling between perpendicular and parallel components of the mode from the governing equations [Eqs. (20) and (21)] for the intermediate nonlinear phase. The governing equations for the intermediate nonlinear regime are derived, and its numerical solutions agree with results from direct MHD simulations of a line-tied g-mode, which covers both the Cowley-Artun regime of early nonlinear phase and the intermediate nonlinear regime. The intermediate nonlinear regime appears to be the major and most relevant nonlinear regime of a line-tied g mode.

Acknowledgments

This research is supported by U.S. Department of Energy under Grant No. DE-FG02-86ER53218. Computations were performed in National Energy Research Scientific Computing Center, which is supported by U.S. Department of Energy under Contract No. DE-AC03-76SF00098, and on the Zaphod Beowulf cluster which was in part funded by the Major Research Instrumentation program of the National Science Foundation under grant ATM-0420905. The authors are grateful for discussions with J. D. Callen, and S. C. Cowley.

[1] C. C. Hegna, J. W. Connor, R. J. Hastie, and H. R. Wilson, Phys. Plasmas **3**, 584 (1996).

[2] P. B. Snyder, H. R. Wilson, J. R. Ferron, L. L. Lao, A. W. Leonard, T. H. Osborne, A. D. Turnbull, D. Mossessian, M. Murakami, and X. Q. Xu, Phys. Plasmas **9**, 2037 (2002).

[3] A. Kirk, B. Koch, R. Scannell, H. R. Wilson, G. Counsell, J. Dowling, A. Herrmann, R. Martin, and M. W. (the MAST team), Phys. Rev. Lett. **96**, 185001 (2006).

[4] D. Brennan, E. Held, S. Kruger, A. Pankin, D. Schnack, and C. Sovinec, Report UW-CPTC 05-8, University of Wisconsin-Madison (2005).

[5] J. W. Connor, R. J. Hastie, and J. B. Taylor, Proc. R. Soc. Lond. A. **365**, 1 (1979).

[6] R. L. Dewar and A. H. Glasser, Phys. Fluids **26**, 3038 (1983).

[7] P. Zhu, A. Bhattacharjee, and K. Germaschewski, Phys. Rev. Lett. **96**, 065001 (2006).

[8] D. Pfirsch and R. N. Sudan, Phys. Fluids B **5**, 2052 (1993).

[9] S. C. Cowley and M. Artun, Phys. Rep. **283**, 185 (1997).

[10] P. Zhu, C. C. Hegna, and C. R. Sovinec, Phys. Plasmas **13**, 102307 (2006).

[11] C. Sovinec, A. Glasser, D. Barnes, T. Gianakon, R. Nebel, S. Kruger, D. Schnack, S. Plimpton, A. Tarditi, M. Chu, et al., J. Comput.Phys. **195**, 355 (2004).

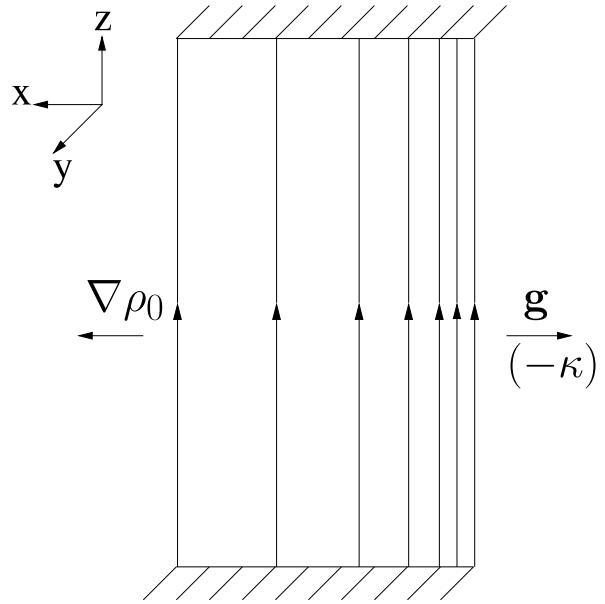

FIG. 1: A shearless slab configuration of line-tied flux tubes. The gravity **g** here is equivalent to the magnetic curvature $-\kappa$ in a curved magnetic configuration.

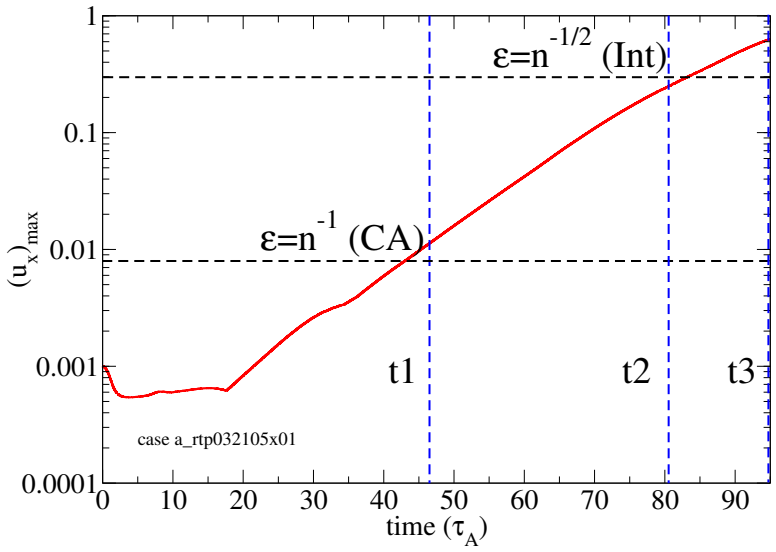

(a)

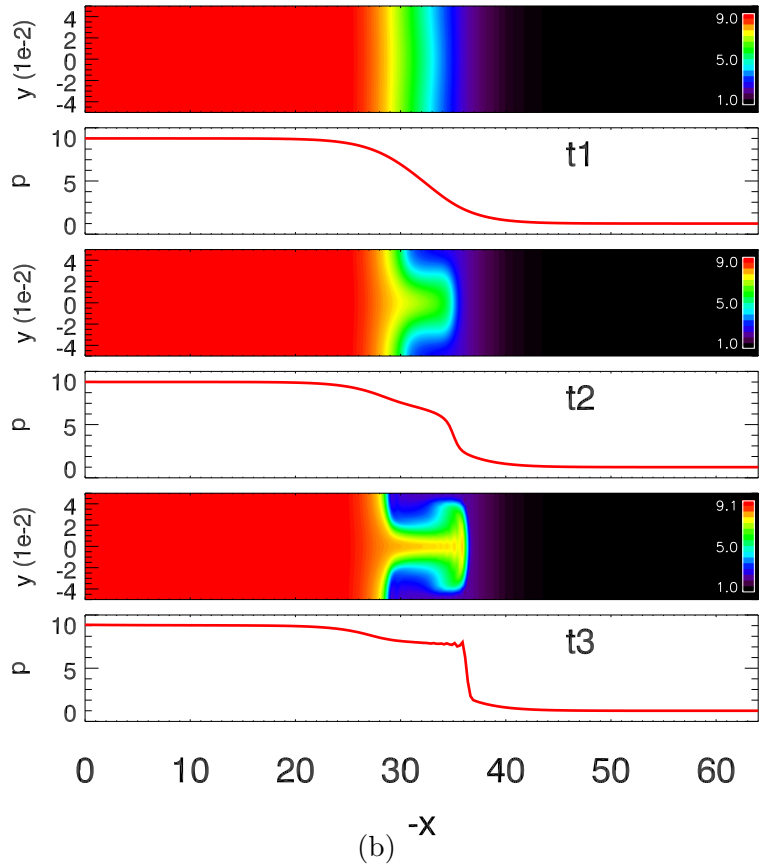

(b)

FIG. 2: (a) Growth of the maximum of flow in x direction in a direct MHD simulation of a line-tied g mode. The maximum amplitude of the initial velocity perturbation is 10^{-3}. The two horizontal broken lines mark the CA regime and the intermediate regime respectively; the three vertical broken lines represent the three time slices at which the pressure contours and profiles are plotted in (b). (b) Pressure contours in $x-y(z=0)$ plane and pressure profile along $x(y=z=0)$ at three time slices $t=t_1,t_2,t_3$ respectivly.

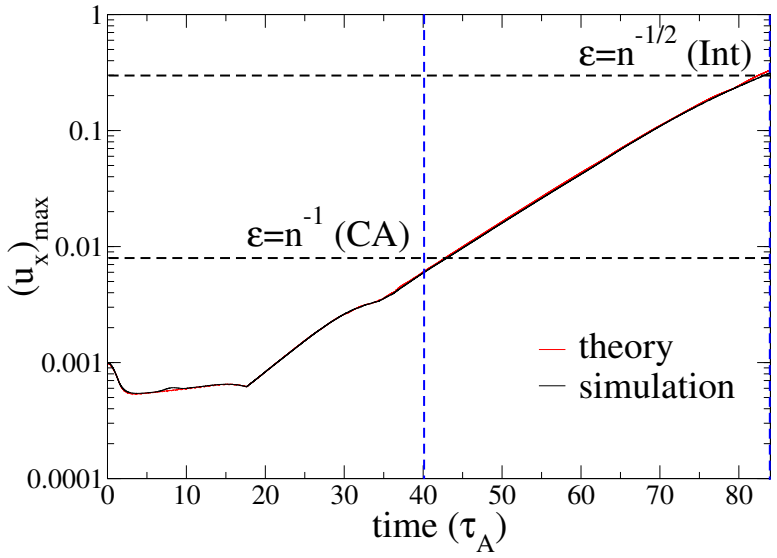

FIG. 3: Growth of the maximum of flow in x direction obtained from theory (red) and simulation (black). The maximum of the initial flow is $u_{x0} = 10^{-3}$. The two horizontal (vertical) broken lines represent the CA regime and the intermediate regime in mode magnitude (in time) respectively.

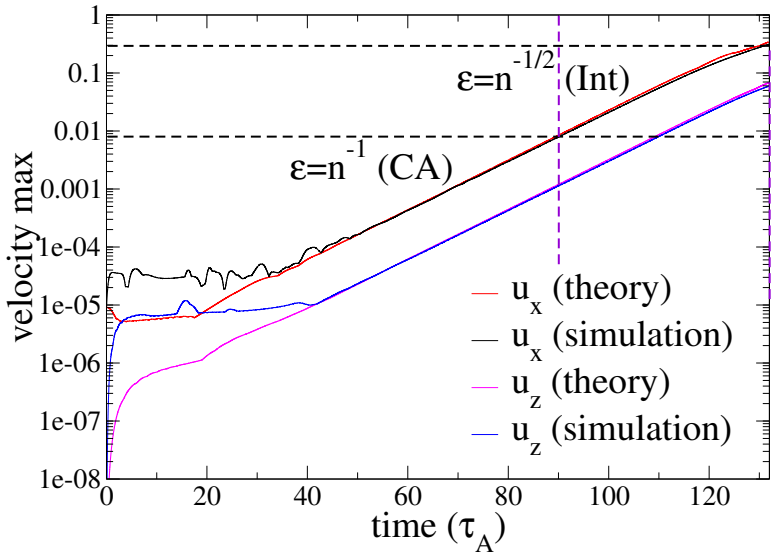

FIG. 4: Growth of the maximum of flow obtained from theory (x-component: red; z-component: magenta) and from simulation (x-component: black; z-component: blue). The maximum of the initial flow is $u_{x0} = 10^{-5}$. The two horizontal (vertical) broken lines represent the CA regime and the intermediate regime in mode magnitude (in time) respectively.